596 *KSME International Journal, Vol. 13, No. 9, pp. 596~608, 1999*

Dynamic Response and Damage of Composite Shell Under Impact

Chongdu Cho* and Guiping Zhao**

(Received November 11, 1998)

The dynamic response and damage of laminated composite cylindrical shell subjected to impact load is numerically investigated using the finite element method. A nine-node isoparametric quadrilateral element based on Sander's shell theory is developed, in which the transverse shear deformation is considered. A semi-empirical contact law that accounts for the permanent indentation is incorporated into the finite element program to evaluate the contact force. The Newmark time integration algorithm is used for solving the time dependent equations of the shell and the impactor. The Tsai-Wu failure criterion is used to estimate the failure of the laminated shell. Numerical results, including the contact force history, interlaminate damage zone, and failure indices in the shell are presented. Effects of curvature, impact velocity and mass of impactor on the composite shell behaviors are discussed.

Key Words: Composite Shell, Impact, Finite Element Analysis, Damage

1. Introduction

Composite materials have been widely utilized in engineering structures. The impact problem is one of the major concerns in designing composite -made structures. In certain circumstances, impact can cause severe damages in composite structures and results in internal and/or external failure of the structures such as matrix cracking, fiber breakage, and delamination. Research works have been actively developed on impact problems of the composite laminates.

Sun and Chen (1985) studied the impact on initially stressed or buckled composite plates. An empirical contact law (Tan and Sun, 1985) for simulating the contact force of a projectile on the impacted composites was developed. Aggour and Sun (1988) applied the contact law by Yang and Sun (1982) to the finite element analysis and showed the result corresponding to their experiment results. Besides, dynamic large deflection of composite laminates impacted by a hard object was investigated and the nonlinear effect was discussed (Chen and Sun, 1985).

Several analytical models (Shivakumar, Elber and Illg, 1985; Choi and Hong, 1994) including spring-mass model and energy-balance model, were developed to study the transient dynamic response and damage of composites due to impact. A method (Wu and Yen, 1994) that predicted contact mechanics between composite laminates and rigid spheres was derived by the three-dimensional anisotropic elasticity theory. Some impact tests (Wu and Springer, 1988) were procured for obtaining detail data that could be used to verify models describing impact-induced damage in the composite plates.

Wu and Chang (1989) studied the strain energy density distributions in the laminated plate as a function of time and reported that a correlation existed between the strain energy density distribution and impact damage.

Choi *et al.* (1991) analyzed the impact damage mechanism and mechanics of graphite/epoxy laminated composites. The impact damage of graphite/epoxy laminated composites in terms of matrix cracking and delaminations resulting from a point-nose impactor (Choi and Chang, 1992)

* Associate professor, School of Mechanical, Aerospace, and Automation Engineering, Inha University, 253 Yong Hyun, Nam Ku, Inchon, Korea

** Graduate student, Inha University, 253 Yong Hyun, Nam Ku, Inchon, Korea

or a line-nose impactor (Choi, Wang and Chang, 1992) were concerned. The results of the predictions agreed to the experiments.

Lee and Park (1990) employed a C^0 continuous displacement finite element method based on a higher-order shear deformation theory to predict the transient response of laminated composite plates subjected to low-velocity impact. Comparisons of numerical results using the higher order theory and the first order theory have shown that the higher order theory provides more accurate results.

Kim, M.S., Kim, N.S. and Lee, H.C. (1991) did an impact test of the plate of composite materials and analyzed the impulsive stress and wave propagation of the laminated composite plates subjected to the transverse low-velocity impact of a steel ball by the finite element method. The results obtained by theory were in good agreement with those by experiment.

Choi and Hong (1993) developed a finite element formulation considering higher order shear deformation and large deflection of the laminated plate and investigated the low-velocity impact response of a composite laminated plate.

However most of the researches have focused on the laminated composite plate and beam structures, while relatively few researches have been carried out on laminated composite shell structures. In the fact, the most composite structures, such as pressure vessels, pipelines, rocket motor casing, etc. are rarely completely flat in practice. So dynamic response and damage analysis about laminated composite shell would be of more significance.

Some of the recent studies have been done on dynamics of non-planar composite structures. Christoforou *et al.* (1989; 1990) conducted experiment and model studies of the cylinders under impact. Christoforou and Swanson (1990) carried out a combined experimental-analytical study using instrumented drop-weight impact of cylindrical tubes. Two analytic models were presented. First one is a simple spring-mass model to calculate the impact response of the empty cylinders. The other is a ring model based on an energy method. The response of the ring was calculated by the strength of materials approach. An analytical solution (Christoforou, Swanson and Beckwith, 1989) was given for the problem of simply supported orthotropic cylindrical shell subjected to impact loading by neglecting in-plane and rotary inertia. The analysis was based on Love's first-approximation shell theory, in which the transverse shear deformation was neglected. However, the application of such theories to layered anisotropic composite shells could lead to 30% or more error (Reddy, 1992) in deflections and stresses.

Ramkumar and Thakar (1987) studied the impact response of curved laminated plates, using Donnel's approximations for thin shells. In their study, the coupled governing equations, in terms of the Airy stress function and shell deformation, were solved using Fourier series expansions. Closed-form analytical solution for curved laminated plate deflections and strains were obtained. But, for reducing governing differential equation, rotational inertia effects and in-plane effects were assumed to be negligible compared to flexural effects. The contact force history due to the impact phenomenon was assumed to be a known input to the analysis, i.e. on the assumption that the impact force varied linearly with time and acted uniformly over a constant area surrounding the impact location.

Lee, Y.S. and Lee, K.D. (1997) investigated the free vibration and dynamic response of cross-ply for CFRP and GFRP laminated cylindrical shell under loads of step pulse, sine pulse triangular pulse and exponential pulse. The analysis was based on an expansion of the loads, displacements and rotations in a double Fourier series. The results concluded that dynamic responses were governed primarily by the natural period of the structure.

In this paper, the dynamic behavior and interlaminar damage of graphite/epoxy laminated cylindrical shell impacted by a hard object are investigated by using the finite element method. In order to calculate the contact force, an experimentally established contact law (Tan and Sun, 1985), which accounts for the permanent indentation is employed. The finite element equations are

solved using the Newmark time integration algorithm in conjunction with successive iterations within each time step. The Tsai-Wu failure criterion of the composite material is used to estimate the damage zone of the cylindrical shell. The different damage mechanism between the plate and the finite curvature shell are analyzed. Numerical results, including the contact force history, deflection, and failure contours in the shell are obtained. The influence of curvature, impact velocity, and mass of impactor are discussed.

2. General Theory

2.1 Virtual work of impact system

The cylindrical shell under consideration is made of thin homogeneous orthotropic layers, oriented arbitrarily and having a total thickness h and mid-surface radius R, as shown in Fig. 1(a). Let the x-θ coordinates coincide with the mid-surface of the cylindrical shell with the z-axis oriented in the thickness direction. In shear deformation theory of the shell, involving 5 degrees of freedom, i.e. the displacement components u, v, w in the x, θ, and z directions, respectively; and rotation of the cross-sections ϕ_x, ϕ_θ about the θ and x axes respectively, of which positive direction is shown in Fig. 1(b), the displacement components of a laminated shell are of the form

$$\begin{aligned} u(x, \theta, z, t) &= u_0(x, \theta, t) + z\phi_x(x, \theta, t) \\ v(x, \theta, z, t) &= v_0(x, \theta, t)(1 + z/R) \\ &\quad + z\phi_\theta(x, \theta, t) \\ w(x, \theta, z, t) &= w_0(x, \theta, t) \end{aligned} \tag{1}$$

where u_0, v_0, and w_0 are corresponding mid-surface displacements in the x, θ, and z directions, respectively and t denotes time variable.

The strain-displacement relation of an orthogonal curvilinear coordinates system are given as

$$\begin{aligned} \varepsilon_x &= \partial u_0/\partial x + z(\partial\phi_x/\partial x) = \varepsilon_x^0 + z\chi_x \\ \varepsilon_\theta &= \partial v_0/\partial\theta + w/R + z(\partial\phi_\theta/\partial\theta) \\ &= \varepsilon_\theta^0 + z\chi_\theta \\ \gamma_{x\theta} &= \partial v_0/\partial x + \partial u_0/\partial\theta + z[\partial\phi_\theta/\partial x \\ &\quad + \partial\phi_x/\partial\theta + (\partial v_0/\partial x - \partial u_0/\partial\theta)/(2R)] \\ &= \gamma_{x\theta}^0 + z\chi_{x\theta} \\ \gamma_{\theta z} &= \partial w_0/\partial\theta + \phi_\theta - v_0/R = \gamma_{\theta z}^0 \\ \gamma_{xz} &= \partial w_0/\partial x + \phi_x = \gamma_{xz}^0 \end{aligned} \tag{2}$$

where ε_i^0 and γ_{ij}^0 are the mid-surface normal strains and shear strains, respectively. χ_i, and χ_{ij} are the curvature and twist changes, respectively. The dimension of θ coordinate is length, i.e. $d\theta = Rd\alpha$.

The stress resultants can be expressed as

$$\begin{aligned} (N_x, N_\theta, N_{x\theta}) &= \int_{-h/2}^{h/2} (\sigma_x, \sigma_\theta, \sigma_{x\theta})\, dz \\ (M_x, M_\theta, M_{x\theta}) &= \int_{-h/2}^{h/2} (\sigma_x, \sigma_\theta, \sigma_{x\theta})\, z dz \\ (Q_{\theta z}, Q_{xz}) &= \int_{-h/2}^{h/2} (\sigma_{\theta z}, \sigma_{xz})\, dz \end{aligned} \tag{3}$$

where N_i, N_{ij} and M_i, M_{ij} are inplane stress resultants and stress couples, respectively; Q_{ij} are the shear stress resultants; and positive directions

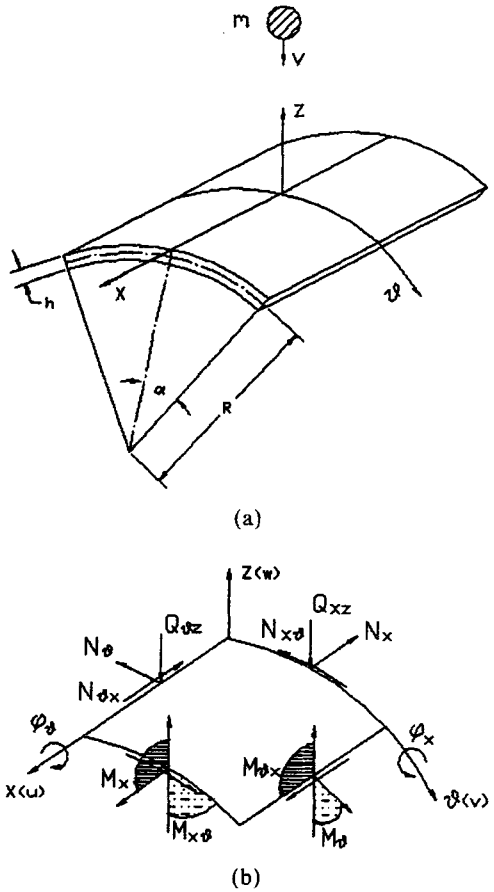

Fig. 1 System configuration and cylindrical coordinates

of these stress resultants are shown in Fig. 1 (b).

The constitutive equations of individual lamina are of the form

$$\{\sigma\}=[C^m]\{\varepsilon\} \tag{4}$$

where $[C^m]$ are the stiffness matrix of the m-th ply in the shell. Substitution of Eq. (4) into Eq. (3) gives

$$\begin{Bmatrix} N_x \\ N_\theta \\ N_{x\theta} \end{Bmatrix}=\begin{bmatrix} A_{11} & A_{12} & A_{16} \\ A_{12} & A_{22} & A_{26} \\ A_{16} & A_{26} & A_{66} \end{bmatrix}\begin{Bmatrix} \varepsilon_x^0 \\ \varepsilon_\theta^0 \\ \gamma_{x\theta}^0 \end{Bmatrix}+\begin{bmatrix} B_{11} & B_{12} & B_{16} \\ B_{12} & B_{22} & B_{26} \\ B_{16} & B_{26} & B_{66} \end{bmatrix}\begin{Bmatrix} \chi_x \\ \chi_\theta \\ \chi_{x\theta} \end{Bmatrix} \tag{5}$$

$$\begin{Bmatrix} M_x \\ M_\theta \\ M_{x\theta} \end{Bmatrix}=\begin{bmatrix} B_{11} & B_{12} & B_{16} \\ B_{12} & B_{22} & B_{26} \\ B_{16} & B_{26} & B_{66} \end{bmatrix}\begin{Bmatrix} \varepsilon_x^0 \\ \varepsilon_\theta^0 \\ \gamma_{x\theta}^0 \end{Bmatrix}+\begin{bmatrix} D_{11} & D_{12} & D_{16} \\ D_{12} & D_{22} & D_{26} \\ D_{16} & D_{26} & D_{66} \end{bmatrix}\begin{Bmatrix} \chi_x \\ \chi_\theta \\ \chi_{x\theta} \end{Bmatrix} \tag{6}$$

$$\begin{Bmatrix} Q_{\theta z} \\ Q_{xz} \end{Bmatrix}=\begin{bmatrix} H_{44} & H_{45} \\ H_{45} & H_{55} \end{bmatrix}\begin{Bmatrix} \gamma_{\theta z}^0 \\ \gamma_{xz}^0 \end{Bmatrix} \tag{7}$$

where A_{ij}, B_{ij}, D_{ij} and H_{ij} are the inplane, coupling, bending, and transverse shear stiffness of the laminated shell, respectively.

$$(A_{ij}, B_{ij}, D_{ij})=\int_{-h/2}^{h/2}(1, z, z^2)\, C_{ij}^m dz \qquad (i, j=1, 2, 6)$$

$$H_{ij}=\int_{-h/2}^{h/2} k_i k_j C_{ij}^m dz \qquad (i, j=4, 5)$$

where k_i, and k_j are the shear correction factors.

The equilibrium configurations of the system consisting of the cylindrical shell and the impactor at initial contact and time t are shown in Fig. 2. The principle of virtual work for the system at time $t+\Delta t$ is written as follows

$$\int_{-h/2}^{h/2}\Big\{\int_\Omega(\sigma_x\delta\varepsilon_x+\sigma_\theta\delta\varepsilon_\theta+\sigma_{x\theta}\delta\gamma_{x\theta}+\sigma_{\theta z}\delta\gamma_{\theta z}+\sigma_{xz}\delta\gamma_{xz}+\rho[\ddot{u}+z\ddot{\phi}_x][\delta u+z\delta\phi_x]+\rho[(1+z/R)\,\ddot{v}+z\ddot{\phi}\theta][(1+z/R)\,\delta v+z\delta\phi_\theta]+\rho\ddot{w}\delta w)\,dxd\theta)\,dxd\theta\}dz+\delta w_i m_i\ddot{w}_i+F\delta\alpha=0 \tag{8}$$

where ρ is the density of the laminated shell.

Substituting Eqs. (2) ~ (7) into the virtual work principle, Eq. (8) can be rewritten as

$$\int_\Omega\{N_x\delta\varepsilon_x^0+N_\theta\delta\varepsilon_\theta^0+N_{x\theta}\delta\gamma_{x\theta}^0+M_x\delta\chi_x+M_\theta\delta\chi_\theta+M_{x\theta}\delta\chi_{x\theta}+Q_{\theta z}\delta\gamma_{\theta z}^0+Q_{xz}\delta\gamma_{xz}^0+(I_1\ddot{u}+I_2\ddot{\phi}_x)\cdot\delta u+\Big[(I_1+2I_2/R)\,\ddot{v}+(I_2+I_3/R)\,\ddot{\phi}_\theta\Big]\delta v+I_1\ddot{w}\delta w+(I_3\ddot{\phi}_x+I_2\ddot{u})\,\delta\phi_x+[I_3\ddot{\phi}_\theta+(I_2+I_3/R)\,\ddot{v}]\delta\phi_\theta\}dxd\theta+\delta w_i m_i\ddot{w}_i+F\delta\alpha=0 \tag{9}$$

where I_i is the inertia defined as

$$(I_1, I_2, I_3)=\int_{-h/2}^{h/2}\rho(1, z, z^2)\,dz$$

In Eqs. (8) and (9), m_i, w_i, and $\ddot{w}_i$ are the mass, displacement, and acceleration of the impactor, respectively; F is the contact force between the shell and the impactor; and α is indentation. The indentation is explained in Fig. 2 and expressed by

$$\alpha=w_i(t+\Delta t)-w_s(x_0, \theta_0, t+\Delta t)$$

in which w_s is the shell deflection at the impact point (x_0, θ_0).

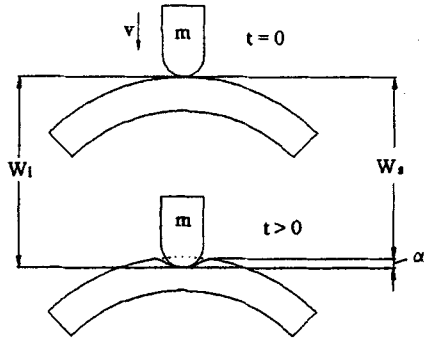

Fig. 2 System configuration before and after impact.

2.2 Finite element formulation

For the finite element model 9-node isoparametric quadrilateral elements are employed. For convenience, a local natural coordinate system (ξ, η, ζ) is shown in Fig. 3. The mid-surface of the shell is subdivided into a number of finite elements. Over the typical shell element, the gener-

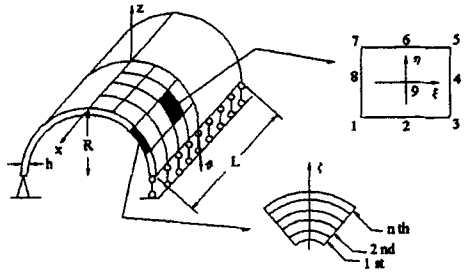

Fig. 3 Global and local coordinates in the cylindrical shell element.

alized displacements (u_0, v_0, w_0, ϕ_x, ϕ_θ) are interpolated by nodal displacements

$$\begin{aligned} u_0(\xi, \eta, t) &= \sum_{i=1}^{9} N_i(\xi, \eta)\, u_{0i}(t) \\ v_0(\xi, \eta, t) &= \sum_{i=1}^{9} N_i(\xi, \eta)\, v_{0i}(t) \\ w_0(\xi, \eta, t) &= \sum_{i=1}^{9} N_i(\xi, \eta)\, w_{0i}(t) \\ \phi_x(\xi, \eta, t) &= \sum_{i=1}^{9} N_i(\xi, \eta)\, \phi_{xi}(t) \\ \phi_\theta(\xi, \eta, t) &= \sum_{i=1}^{9} N_i(\xi, \eta)\, \phi_{\theta i}(t) \end{aligned} \tag{10}$$

where N_i are the interpolation function of Lagrange family quadratic rectangular elements. u_{0i}, v_{0i}, w_{0i}, ϕ_{xi}, and $\phi_{\theta i}$ are nodal point values of u_0, v_0, w_0, ϕ_x, ϕ_θ at i nodal point. The local and global coordinates are related by the following equations

$$\begin{aligned} x &= \sum_{i=1}^{9} N_i(\xi, \eta)\, x_i \\ \theta &= \sum_{i=1}^{9} N_i(\xi, \eta)\, \theta_i \end{aligned} \tag{11}$$

where x_i and θ_i are the global coordinates of the nodal point i.

Substituting of Eq. (10) into the virtual work principle, Eq. (9), with consideration of Eqs. (1), (2) and (5) ~ (7), Eq. (9) can be written as two coupled equations.

$$m_i \ddot{w}_i + F = 0 \tag{12}$$

$$[M]\{\ddot{\Delta}\} + [K]\{\Delta\} = \{F\} \tag{13}$$

where $[M]$ and $[K]$ are the mass and stiffness matrix, $\{\Delta\}$ and $\{F\}$ the generalized displacements vector and the contact force vector. Eq. (12) governs the impactor motion, while Eq. (13) evaluates the shell response.

Because the generalized displacements of the elements are expressed as a function of local coordinates ξ and η, it is necessary to express the generalized displacement derivatives and area integration in terms of ξ and η. This can be done by using the coordinate transformation Eq. (11) and the element Jacobian matrix.

In the numerical integration of the stiffness matrix $[K]$, in order to avoid the shear-locking, selective reduced integration method is employed. The 3×3 Gaussian rule is used to compute the stiffness coefficients for the inplane and bending deformation, and the reduced 2×2 Gaussian rule to compute the stiffness coefficients for the transverse shear deformation.

2.3 Indentation law

Before Eqs. (12) and (13) are solved, the contact force, F, between the impactor and the laminate shell must first be found. The evaluation of the contact force depends on a contact law, named Hertzian contact law, which relates the contact force with the indentation. Tan and Sun (1985) proposed a power law based on static indentation tests using steel ball as indentors. This contact law accounts for permanent indentation after unloading. The modified version was used in the study of laminated composite plate by Chen and Sun (1985) as well as Wu and Chang (1989). The modified contact law is given as follows

Loading:

$$F = k\alpha^{1.5} \tag{14}$$

Unloading:

$$F = F_m\left(\frac{\alpha - \alpha_0}{\alpha_m - \alpha_0}\right)^q \tag{15}$$

Reloading:

$$F = F_m\left(\frac{\alpha - \alpha_0}{\alpha_m - \alpha_0}\right)^{1.5} \tag{16}$$

In the above equations, α_m is the maximum indentation during loading, F_m is the maximum contact force at the beginning of unloading, α_0 denotes the permanent indentation in a loading-unloading cycle and is given by

$$\alpha_0 = \begin{cases} \beta(\alpha_m - \alpha_p) & \text{if}(\alpha_m > \alpha_p) \\ 0 & \text{if}(\alpha_m < \alpha_p) \end{cases} \tag{17}$$

in which α_p and β were constants determined by the experiment. α_p could be considered as a critical value of indentation beyond which permanent deformation would occur and β as a coefficient expressing a linear relationship between the permanent indentation α_0 and the corresponding maximum indentation α_m. For the spherical steel indenter of diameter 1.27 cm and Graphite/epoxy laminated plate, α_p and β were found to be 1.667×10^{-2} cm and 0.094 from test data using least-squares fitting method, the contact coeffi-

cient k and power index q of the unloading law were found to be 1.413×10^6 N/cm$^{1.5}$ and 2.5, respectively (Tan and Sun, 1985).

In the present study, the contact laws given by Eqs. (14) ~ (16) are incorporated into Eqs. (12) and (13) to solve the impact response. In addition, the contact force history, the deflection of the laminated composite cylindrical shell and the displacement of the impactor are obtained.

2.4 Solution algorithm

A couple of Eqs. (12) and (13) combined with the contact law given by Eqs. (14) ~ (16) can be solved simultaneously. The Newmark constant -acceleration time-integration algorithm is used in the present analysis,

$$\{\dot{\Delta}\}_{t+\Delta t}=\{\dot{\Delta}\}_t+[(1-\alpha_1)\{\ddot{\Delta}\}_t+\alpha_1\{\ddot{\Delta}\}_{t+\Delta t}]\Delta t$$
$$\{\ddot{\Delta}\}_{t+\Delta t}=A_0[\{\Delta\}_{t+\Delta t}-\{\Delta\}_t]-A_1\{\dot{\Delta}\}_t-A_2\{\ddot{\Delta}\}_t \tag{18}$$

where

$$A_0=1/\alpha_2\Delta t^2$$
$$A_1=1/\alpha_2\Delta t$$
$$A_2=1/2\alpha_2-1$$

In Eq. (18), Δt is the time step, and the parameters α_1 and α_2 can be determined to obtain integration accuracy and stability. For $\alpha_1=0.5$ and $\alpha_2=0.25$, this method is unconditionally stable for time step. At time $t+\Delta t$, Eq. (13) may be expressed in the iteration form as

$$[\tilde{K}]\{\Delta\}^{i+1}_{t+\Delta t}=\frac{\Delta t^2}{4}\{F\}^i_{t+\Delta t}+[M]\{b\}_t \tag{19}$$

where

$$\{b\}_t=\{\Delta\}_t+\Delta t\{\dot{\Delta}\}_t+\frac{\Delta t^2}{4}\{\ddot{\Delta}\}_t$$
$$[\tilde{K}]=\frac{\Delta t^2}{4}[K]+[M]$$

In Eq. (19), i is the number of iterations within a time step. The same solution scheme is used for solving the equation of motion of the impactor as a rigid body, i.e. Eq. (12). Successive iteration continues until a solution of the desired accuracy is reached in each time step. Note that a modified contact force $F^i_{t+\Delta t}$ obtained from the previous iteration is used for the current response.

2.5 Failure criterion

In order to predict the occurrence of the damage in the shell by impact, Tsai and Wu failure theory was employed. In the Tsai-Wu general quadratic interaction criteria, the failure surface in stress space is described by the tensor polynomial

$$F_i\sigma_i+F_{ij}\sigma_i\sigma_j=1 \tag{20}$$

where the contracted notation $i, j=1, 2, \ldots 6$ is used and F_i and F_{ij} are the experimentally determined strength tensors of the second and fourth rank, respectively. For the case of plane stress, Eq. (20) reduces to

$$F_1\sigma_1+F_2\sigma_2+F_{11}\sigma_1^2+F_{66}\sigma_2^2+F_{11}\sigma_6^2+2F_{12}\sigma_1\sigma_2=1 \tag{21}$$

where σ_1, σ_2, and σ_6 are normal and shear stress components along the principle material axes. F_i and F_{ij} are strength tensors. With the exception of F_{12}, all the strength tensors can be expressed in terms of the uniaxial and shear strengths in Eq. (21). For F_{12}, it would be proposed to take on the form of function of the F_{11} and F_{22} approximately (Gibson, 1994).

$$\begin{aligned}
F_{11}&=\frac{1}{S_L^+S_L^-}\\
F_1&=\frac{1}{S_L^+}-\frac{1}{S_L^-}\\
F_{22}&=\frac{1}{S_T^+S_T^-}\\
F_2&=\frac{1}{S_T^+}-\frac{1}{S_T^-}\\
F_{66}&=\frac{1}{S_{LT}^2}\\
F_{12}&=-\frac{(F_{11}F_{12})^{1/2}}{2}
\end{aligned} \tag{22}$$

where S_L^+ and S_L^- are the longitudinal tensile and compressive strengths of the lamina; S_T^+ and S_T^- are the transverse strengths of the lamina; S_{LT} is the in-plane shear strength. The terms of the left-hand side of Eq. (21) are regarded as failure index. We assumes the damage zone for which stress states are predicted to exceed the allowable value, i. e. failure is predicted when the failure index is exceeding unit. Maximum failure index is the largest one of the failure indices estimated in the ply. It means the first failure appears in this

point of the ply.

In the present analysis, 9-node isoparametic element is used. The element stresses of the m-th layer at Gaussian points, can be calculated using the relation

$$\{\sigma\}^{e}_{Gauss}=[C^m](\{\varepsilon^0\}+\zeta\{\chi\}) \tag{23}$$

where $[C^m]$ is defined in Eq. (4) and ζ is shown in Fig. 3.

To estimate failure zone of the elements, nodal stresses of the elements, $\{\sigma\}^m_{nodes}$, need to be known. We can use the least squares procedure (Bathe, 1996) to calculate the values $\{\sigma\}^m_{noden}$ by minimizing the errors between the given integration point values $\{\sigma\}^e_{Gauss}$ and the values $\{\sigma\}^c_{Gauss}$ calculated at the same points by interpolation from the nodal point values $\{\sigma\}^m_{noden}$. The errors can be symbolized as

$$\{\Phi\}=\{\sigma\}^e_{Gauss}-\{\sigma\}^c_{Gauss} \tag{24}$$

where $\{\sigma\}^c_{Gauss}$ is calculated by interpolation function $[N]$

$$\{\sigma\}^c_{Gauss}=[N]\{\sigma\}^m_{nodes} \tag{25}$$

Let the functional of the errors (Wang and Wu, 1997)

$$I=\int_v\{\Phi\}^T\{\Phi\}dv \tag{26}$$

Take the stationary value of the functional I

$$\frac{\partial I}{\partial\{\sigma\}^m_{nodes}}=\{0\} \tag{27}$$

We obtain

$$[k]\{\sigma\}^m_{nodes}=\{f\} \tag{28}$$

where

$$[k]=\int_{-1}^{1}\int_{-1}^{1}\int_{-h/2}^{h/2}[N]^T[N]\det[J]d\xi d\eta d\zeta$$

$$\{f\}=\int_{-1}^{1}\int_{-1}^{1}\int_{-h/2}^{h/2}[N]^T[C^m](\{\varepsilon^0\}+\zeta\{\chi\})\det \cdot[J]d\xi d\eta d\zeta$$

In above expressions $[J]$ is Jacobian matrix. To solve Eq. (28), the *m-th* layer lamina nodal stresses can be obtained. The lamina nodal stresses can be used in conjunction with a lamina strength criterion, Eq. (21) to check each lamina against failure.

3. Numerical Results and Discussion

As stated above, a finite element approach has been presented to solve the contact force histories, deflection, and strains in the shell, and to estimate the failure zone and contour of the damage in a composite cylinder subjected to lateral impact loading. The resulting expressions have been coded into a C language program and a dynamic analysis and failure prediction can be accomplished.

3.1 Numerical example

The composite cylindrical shell considered is 20-plied $[0/45/0/-45/0]_{2s}$ Graphite/Epoxy laminated shell with radius R, length L, and thickness h, as in Fig. 3. The cylindrical shell is assumed to impacted normally at the center by a steel impactor with a contacting spherical cap of diameter 1.27 cm. The shell along the edge is simply supported. One quarter of the shell is analyzed because of the symmetry in the laminate geometry, loading, and boundary condition. The material properties of the composite cylindrical shell for the study are listed to be in the Table 1. The failure values for this composite system are assumed in the Table 2.

We first consider that the radius of curvature of the shell is infinite, and then the composite laminate become plate. For checking program validity, the infinite radius case is compared with the results calculated by Chen and Sun (1985). As

Table 1 Elastic properties of a Graphite/Epoxy lamina. (Chen and Sun, 1985)

$E_1=120$ GPa	$E_2=7.9$ GPa
$G_{12}=G_{23}=G_{13}=5.5$ GPa	
$\nu_{12}=0.3$	
$\rho=1.58\times10^{-5}$Ns^2/cm^4	

Table 2 Failure properties for T300/5208 Graphite/Epoxy. (Glbson, 1994)

S^+_L(MPa)	S^-_L(MPa)	S^+_T(MPa)	S^-_T(MPa)	S_{LT}(MPa)
1448	1448	44.8	248	62.1

mentioned by Chen and Sun, (1985), the impact velocity of the impactor of mass 1.96×10^{-4}Ns^2/cm is considered at 30m/s. The finite element meshes used are 4×4 in one quadrant of the laminate with dimension $15.24\times10.16\times0.269$ cm. The corresponding time increments are chosen as 0.2 μs here. Shear correction factors are $k_1=0.864$, and $k_2=0.879$ (Whitney, 1988). The solutions for the contact force and the plate deflection are plotted in Figs. 4 and 5. From the comparison in the Figs. 4 and 5, it can be seen that both Chen and Sun (1985) and this paper are in a good agreement each other.

We next consider a finite radius of curvature with a magnitude R and the same calculation condition is used in the following analysis.

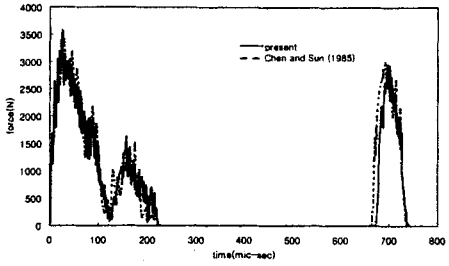

Fig. 4 Contact force histories of the present and Chen and Sun (1985).

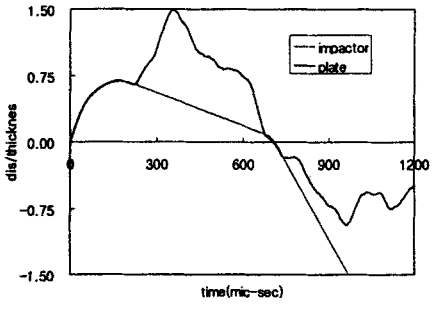

(a)

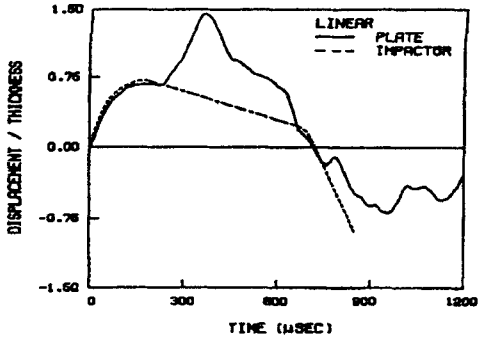

(b)

Fig. 5 Motions of the plate and the impactor (a) the present study; (b) Chen and Sun (1985).

3.2 Results and discussion

Figure 6 shows the contact force versus time responses for the different curvature radii $R=$ 50mm, 100mm, and 10^{30}mm (infinity), at impact velocity $v=20$m/sec. It is evident in Fig. 6 that the contact duration and peak contact force are affected by the curvature radius of the shell. The amplitude of response increases with a decrease in radius of curvature.

Since the stiffness becomes smaller by increasing the curvature radius, the impact duration becomes larger. This result shows that the stiffness and the curvature radius of the shell severely influence the dynamic impact response.

One point worthy of noting is that the contact force is zero during impact indicating that the laminate plate and the impactor are separate after first contact; then they come in contact again

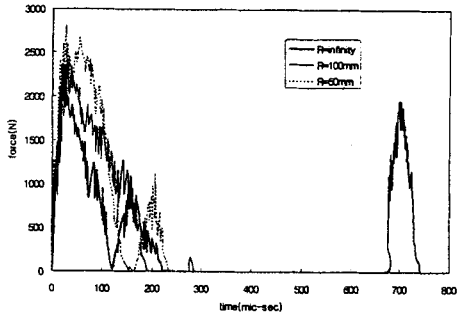

Fig. 6 Comparison of contact force on $R=50$mm, 100mm, and infinity.

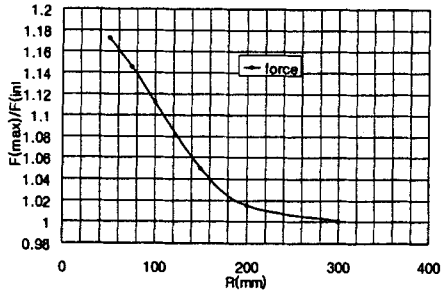

Fig. 7 Curvature effect on maximum contact force.

after the motion of the laminate reverses its direction and snaps back. But this phenomenon does not appear in the shell responses. In the other words, in the plate, the contact between impactor and the laminate occurs two times, in the shells it occurs only once. This means that the impactor keeps on contacting the shells during the whole impact duration.

Figure 7 shows the effects of the curvature radii change on maximum force.

In the laminated composite shell with the same radius of curvature, the contact forces and the shell responses corresponding to different initial impact velocities v are found to be similar except for the amplitude which is approximately proportional to the initial impact velocity. In the other words, the period of contact remains the same. Figure 8 shows the contact force histories of the shell, with the $R=100$mm, impacted by the impactor with initial velocity $v=5$m/sec, 10m/sec, and 20m/sec, respectively.

It is noted that for the impact velocity considered, in the low speed, the contact force was found to be smooth comparatively. While increasing the initial velocity, the contact force fluctuates quite bit. These fluctuations could be caused by the participation of more waves of shorter wavelengths included by the higher impact velocity (Sun and Chen, 1985).

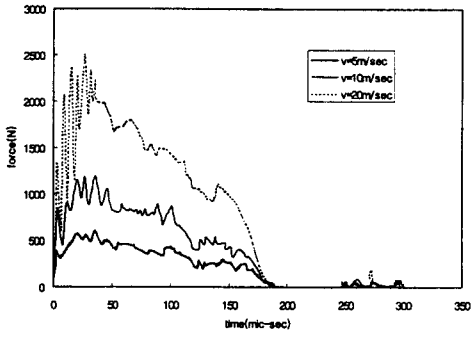

Fig. 8 Contact force histories for different initial velocities.

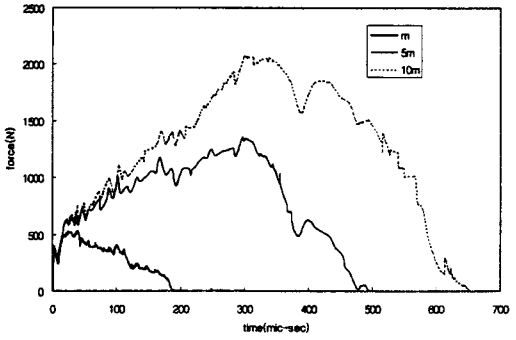

Fig. 9 Contact force for various impactor mass.

When the radius of curvature is kept constant and mass of the impactor is changed, it is found that larger impactor masses cause higher contact force and longer contact time. Figure 9 shows contact force histories for the laminated shell with the radius $R=100$mm subjected to impact of various impactor masses with impact velocity $v=$ 5m/sec, in which mass $m_i=$m, 5m, and 10m (m $=1.96\times10^{-4}$Ns^2/cm), respectively.

It is clear that the response characteristics depend on the ratio of impactor mass to the shell mass.

Maximum failure indices estimated in the shell after impact are listed in the Table 3. Failure index that exceeds unit means damage occurring in this point. Maximum failure index is the maximum one of the failure indices of all the points in the ply. It means the first failure appears in this point of the ply. From Table 3 we can see that the tendency of damage is different between the plate and the shell. It is possible to deduce (Cho and Yoo, 1996) the result from the observation of the shell geometric shape. Under loading, the shell structure makes load redistribute unlike the general plate structure due to the occurrence of compressive reaction. The plate subjected to lateral impact would mainly endure bending so first failure appears at the bottom, e. g. at the 1st ply of bottom surface. The shell impacted by impactor, for internal inplane pressure existed, the internal force distribution state is different from plate, the first ply failure occurs at the top surface of the shell, i. e. the 20th ply, at the situation of the contact point.

It can be seen from Table 3 that each ply failure index of above the mid-surface has a remarkable feature. Maximum failure indices with orientation 45° ply are evidently less than with orientation 0° ply lamina. In general, the failure index predicted depends on the ply properties and stacking

Table 3 Maximum failure index in each layer of the shell with different curvature radius.

Ply		Maximum Tsai-Wu Failure Index					
No.	Orientation	R=infinity	R=200mm	R=150mm	R=100mm	R=75mm	R=50mm
1	0°	**1.388**	0.30002	0.15831	0.28605	0.39047	0.51377
2	45°	**1.09613**	0.34348	0.36595	0.4104	0.42906	0.54516
3	0°	**1.06884**	0.20224	0.05878	0.14343	0.25406	0.49693
4	−45°	0.8051	0.24099	0.24191	0.26771	0.27302	0.41542
5	0°	0.77045	0.10827	0.04936	0.09882	0.18499	0.38109
6	0°	0.62905	0.06275	0.08078	0.08642	0.16178	0.33746
7	−45°	0.41939	0.09465	0.08002	0.06776	0.10005	0.14424
8	0°	0.36184	0.04011	0.16735	0.18031	0.18334	0.15945
9	45°	0.19614	0.03839	0.04148	0.05614	0.07062	0.11075
10	0°	0.11542	0.10973	0.24873	0.29668	0.32436	0.37781
11	0°	0. 11022	0. 19019	0.32494	0.40555	0.45519	0.57093
12	45°	0.16902	0.17139	0.24053	0.28136	0.29776	0.33046
13	0°	0.31506	0.2668	0.31693	0.50691	0.57584	0.73881
14	−45°	0.31093	0.05219	0.28207	0.38269	0.3954	0.41222
15	0°	0.49912	0.33955	0.40873	0.60078	0.6863	0.88143
16	0°	0.58335	0.37449	0.45265	0.6449	0.73771	0.94328
17	−45°	0.47296	0.36598	0.40617	0.52057	0.52195	0.47757
18	0°	0.73623	0.44146	0.53657	0.72751	0.83289	**1.04803**
19	45°	0.54709	0.43691	0.48227	0.6031	0.59305	0.48296
20	0°	0.86831	0.50458	0.6152	0.80262	0.9179	**1.12754**

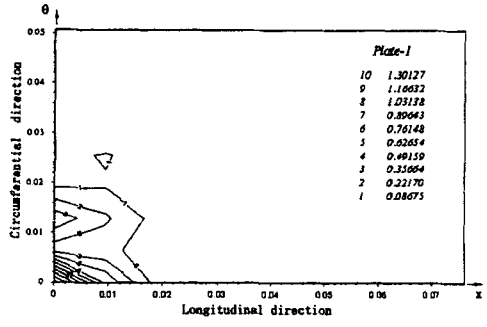

(a) At the 1st ply of the plate;

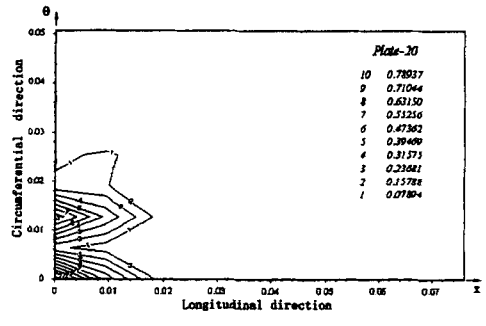

(b) At the 20th ply of the plate;

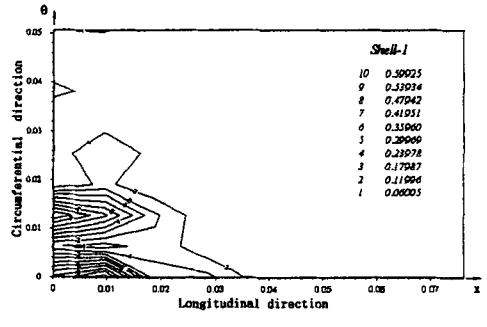

(c) At the 1st ply of the shell;

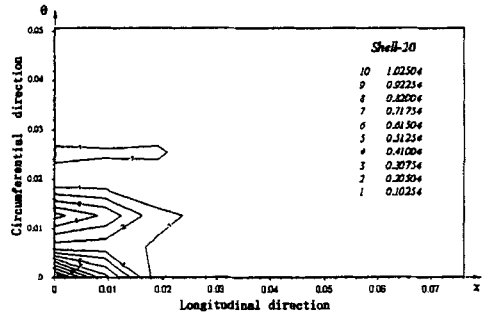

(d) At the 20th ply of the shell.

Fig. 10 Failure contour on the laminate.

sequences.

Figure 10 shows Tsai-Wu failure index contours of the laminates with the infinite curvature and finite curvature ($R=100$mm) at the top and bottom surface, respectively. The legend gives failure indices corresponding to different levels. The difference of maximum index between the plate and shell is found to be significant. In addition, it should be noted that in general there are high-localized stresses associated with the contact point, even when relatively smooth indenters are used. These contact stresses can cause both fiber and matrix damage and lead to strength reductions.

4. Conclusions

In the study, the load distribution of laminated composite cylindrical shell subjected to transverse impact is analyzed. As results, the following are deduced.

(1) The response frequency, or impact duration, is independent of the impact velocity, and depends on the impactor mass, the material properties, and geometrical parameters of the shell.

(2) A large mass of impactor causes higher contact force and increases the contact time. The maximum contact force is 527.1N and contact time 183.5μs for given mass of the impactor. The maximum contact force increases to 2076.1N and contact time 652.1μs when mass of the impactor is 10 times as large as the given mass.

(3) Maximum contact force increases with the decrease of the radius of curvature. The maximum contact force of 300mm radius of courvature shall is 1.0012 times as large as that on the plate. The maximum contact force is 1.172 times for the radius of curvature 50mm.

(4) The position of the first failure is differently estimated between the infinite curvature laminate and finite curvature laminate. The first failure occurs at the bottom surface of the laminate plate and the opposite conclusion for the laminate shell. The maximum failure index is 1.388 at the 1st ply of bottom for the plate and is 1.12754 at the 20th ply of the top surface for the shell.

Acknowledgement

This work was supported by Korea Research Foundation under contract number 1998-018-E00088.

References

(1) Aggour, H. and Sun, C.T., 1988, "Finite Element Analysis of a Laminated Composite Plate Subjected to Circularly Distributed Central Impact Loading," *Computers & Structures*, Vol. 28, No. 6, pp. 729~736.

(2) Bathe, K. J. , 1996, "*Finite Element Procedures*," Prentice-Hall, Inc, pp. 327~330.

(3) Chen, J. K. and Sun, C. T. , 1985, "Analysis of Impact Response of Buckled Composite Laminates," *Composite Structures*, Vol. 3, pp. 97~118.

(4) Chen, J.K. and Sun, C.T., 1985, "Dynamic Large Deflection Response of Composite Laminates Subjected to Impact," *Composite Structures*, Vol. 4, pp. 59~73.

(5) Cho, C.D, Cho, Y.H. and Yoo, B.J., 1996, "Dynamic Response of Laminated Composite Shell under Low-velocity Impact," *Proceedings of 2nd ISIE*, Beijing, China, pp. 312~318.

(6) Choi, H.Y. and Chang, F.K. , 1992, "A Model for Predicting Damage in Graphite/Epoxy Laminated Composites Resulting from Low-Velocity Point Impact," *J. Composite Materials*, Vol. 26, No. 14, pp. 2134~2169.

(7) Choi, H.Y., Downs, R.J. and Chang, F.K., 1991, "A New Approach toward Understanding Damage Mechanisms and Mechanics of Laminated Composite Due to Low-Velocity Impact: Part I - Experiments," *J. Composite Materials*, Vol. 25, pp. 992~1011.

(8) Choi, H.Y., Wang, H.S. and Chang, F.K., 1992, "Effect of Laminate Configuration and Impactor's Mass on the Initial Impact Damage of Graphite/Epoxy Composite Plates Due to Line-Loading Impact," *J. Composite Materials*, Vol. 26, No. 6, pp. 804~827.

(9) Choi, H.Y., Wu, H.Y.T. and Chang, H.K.,

1991, "A New Approach toward Understanding Damage Mechanisms and Mechanics of Laminated Composite Due to Low-Velocity Impact: Part II - Analysis," *J. Composite Materials*, Vol. 25, pp. 1012~1038.

(10) Choi, I.H. and Hong, C.S., 1993, "Low-Velocity Impact Response Analysis of Composite Laminates Considering Higher Order Shear Deformation and Large Deflection," *Trans. of KSME*, Vol. 17, No. 12, pp. 2982~2994.

(11) Choi, I.H. and Hong, C.S., 1994, "New Approach for Simple Prediction of Impact Force History on Composite Laminates," *AIAA J.*, Vol. 32, No. 10, pp. 2067~2072.

(12) Christoforou, A. P. and Swanson, S. R. , 1990, "Analysis of Simply-Supported Orthotropic Cylindrical Shells Subject to Lateral Impact Loads," *J. Applied Mechanics*, Vol. 57, pp. 376~382.

(13) Christoforou, A. P. , Swanson, S. R. and Beckwith, S. W. , 1989, "Lateral Impact of Composite Cylinders," *Composite Materials: Fatigue and Fracture, Second Volume, ASTM STP 1012*, Paul A. Lagace. Ed., American Society for Testing and Materials. Philadelphia, pp. 373~386.

(14) Gibson, R.F. 1994, *Principles of Composite Material Mechanics*, McGraw-Hill, Inc., pp. 108~112.

(15) Hinton, E. and Campbell, J.S., 1979, "Local and Global Smoothing of Discontinuous Finite Element Functions Using Least Squares Method," *Int. J. Numerical Methods in Engineering*, Vol. 8, pp. 461~480.

(16) Lee, Y.S. and Lee, K.D., 1993, "On the Dynamic Response of Laminated Circular Cylindrical Shell under Dynamic Loads," Trans. of KSME, Vol. 17, No. 11, pp. 2684~2693.

(17) Lee, Y.S. and Lee, K.D., 1997, "On the Dynamic Response of Laminated Circular Cylindrical Shell under Impulse Loads," *Computer and structures*, Vol. 63, No. 1, pp. 149~157.

(18) Lee, Y. S. and Park, O., 1990, "Low-Velocity Impact Response of Laminated Composite Plates Using a Higher Order Shear Deformation Theory," *Trans. of KSME*, Vol. 14, No. 6, pp. 1365~1381.

(19) Kim, M.S., Kim, N.S. and Lee, H.C., 1991, "Impact Analysis of Laminated Composite Plates Using Higher-Order Shear Deformation Theory," *Trans. of KSME*, Vol. 15, No. 3, pp. 735~750.

(20) Mindlin, R.D., 1951, "Influence of Rotary Inertia and Shear on Flexural Motions of Isotropic Elastic Plates," *ASME J. Applied Mechanics*, Vol. 18, pp. 31~38.

(21) Ramkumar, R.L. and Thakar, Y.R., 1987, "Dynamic Response of Curved Laminated Plate Subjected to Low Velocity Impact," *J. Engineering Materials and Technology*, Vol. 109, pp. 67~71.

(22) Reddy, J.N., 1992, Energy and Variational Methods in Applied Mechanics. A Wiley-Interscience Publication, pp. 408~410.

(23) Reddy, J.N., 1993, An Introduction to the Finite Element Method, Second Edition, McGraw-Hill, Inc., pp. 411~420.

(24) Shivakumar, K.N., Elber, W. and Illg, W., 1985, "Prediction of Impact Force and Duration Due to Low-Velocity Impact on Circular Composite Laminates," *J. Applied Mechanics*, Vol. 52, pp. 674~680.

(25) Shivakumar, K.N., Elber, W. and Illg, W., 1985, "Prediction of Low-Velocity Impact Damage in Thin Circular Laminates," *AIAA J.*, Vol. 23, No. 3, pp. 442~449.

(26) Sun, C. T. and Chen, J. K., 1985, "On the Impact of Initially Stressed Composite Laminates," *J. Composite Materials*, Vol. 19, pp. 490~504.

(27) Tan, T.M. and Sun, C.T., 1985, "Use of Statical Indentation Law in the Impact Analysis of Laminated Composite Plate," *J. Applied Mechanics*, Vol. 52, pp. 6~12.

(28) Thomas J.R. Hughes., 1987, *The Finite Element Method*, Prentice-Hall, Inc., pp. 327~330.

(29) Wang, H.D. and Wu, D.L., 1997, The Finite Element Method and Compute Program. Architectural Industry Press in China, pp. 101~103.

(30) Whitney, J.M., 1988, "Shear Correction Factors for Orthotropic Laminated Anisotropic Composite Plates," Int. J. of Numerical Methods in Engineering, Vol. 15, pp. 1187~1206.

(31) Wu, E.B. and Yen, C.S., 1994, "The Contact Behavior Between Laminated Composite Plates and Rigid Spheres," *J. Applied Mechanics*, Vol. 61, pp. 60~66.

(32) Wu, H.Y.T. and Chang, F.K., 1989, "Transient Dynamic Analysis of Laminated Composite Plates Subjected to Transverse Impact," *Computers & Structures*, Vol. 31, No. 3, pp. 453~466.

(33) Wu, H.Y.T. and Springer G.S., 1988, "Impact Induced Stresses, Strains, and Delamination in Composite Plates," *J. Composite Materials*, Vol. 22, pp. 533~560.

(34) Wu, H.Y.T. and Springer G.S., 1988, "Measurements of Matrix Cracking and Delamination Caused by Impact on Composite Plates," *J. Composite Materials*, Vol. 22, pp. 518~532.

(35) Yang, S.H. and Sun, C.T., 1982, "Indentation Law for Composite Laminates," *Composite materials: Testing and Design (Sixth Conference), ASTM STP 787*, I. M. Daniel, Ed., American Society for Testing and Materials, pp. 425~449.